

Article

Probabilistically-Shaped DMT for IM-DD Systems with Low-Complexity Fast WHT-Based PDSP

Yi Liu ¹, Haimiao Long ², Ming Chen ^{2,*}, Yun Cheng ¹ and Taoyun Zhou ¹

¹ Department of Information Science and Engineering, Hunan University of Humanities, Science and Technology, Loudi 417000, China

² School of Physics and Electronics, Hunan Normal University, Changsha 410081, China

* Correspondence: ming.chen@hunnu.edu.cn

Abstract: Transmission capacity and receiver sensitivity of an intensity-modulation direct detection (IM-DD) optical discrete multi-tone (DMT) system can be improved by using the probabilistically shaping (PS) technique. However, different probabilistic distributions will be required owing to the unbalanced signal-to-noise ratio (SNR) among data-carrying subcarriers (SCs) induced by the imperfect frequency response of optical/electrical devices, which can increase the implementation complexity of the PS-DMT transceiver. In this work, different signal pre-processing schemes including pre-equalization, Walsh–Hadamard transform (WHT)-based full data-carrying SCs precoding (FDSP) and fast WHT-based partial data-carrying SCs precoding (PDSP) are investigated for SNR equalization in a short-reach PS-DMT transmission system. After transmission over 50 km single-mode fiber, the experimental results indicated that three pre-processed signals have almost the same generalized mutual information (GMI) performance and receiver sensitivity improvements. The proposed fast WHT-based PDSP scheme may be a good option for the implementation of the PS-DMT transmission systems with a large SC SNR fluctuation regarding computational complexity.

Keywords: intensity-modulation and direct-detection (IM-DD); discrete multi-tone (DMT); probabilistically shaping (PS); full data-carrying SC precoding (FDSP); partial data-carrying SC precoding (PDSP); Walsh–Hadamard transform (WHT)



Citation: Liu, Y.; Long, H.; Chen, M.; Cheng, Y.; Zhou, T.

Probabilistically-Shaped DMT for IM-DD Systems with Low-Complexity Fast WHT-Based PDSP. *Photonics* **2022**, *9*, 655. <https://doi.org/10.3390/photonics9090655>

Received: 28 August 2022

Accepted: 12 September 2022

Published: 15 September 2022

Publisher's Note: MDPI stays neutral with regard to jurisdictional claims in published maps and institutional affiliations.



Copyright: © 2022 by the authors. Licensee MDPI, Basel, Switzerland. This article is an open access article distributed under the terms and conditions of the Creative Commons Attribution (CC BY) license (<https://creativecommons.org/licenses/by/4.0/>).

1. Introduction

Intensity-modulation and direct detection (IM-DD) optical discrete multi-tone (DMT) has been widely considered a promising candidate for optical fiber access networks, owing to its high spectral efficiency (SE), robustness against fiber dispersions, and low cost [1–3]. However, current optical access networks cannot support further mobile traffic and keep up with the continuously increased bandwidth demand [4,5]. Thus, one effective scheme named probabilistically shaping (PS) technique has been investigated widely in optical transmission systems due to the improved transmission capacity and receiver sensitivity [6,7]. In [8], the authors proposed a fixed-length matcher named constant composition distribution matching (CCDM), and its output data sequence can obey the same empirical distribution (ED). Moreover, the shaped symbols can be represented by using binary tags and encoded by using forward error correction (FEC) code with preserving the distribution of the shaped symbols. Unfortunately, the practical IM-DD DMT transmission systems suffer the large data-carrying subcarriers (SCs) signal-to-noise ratio (SNR) fluctuation caused by various interferences, such as the data converters-induced clock tone leakage (CTL), imperfect optoelectronic devices-induced nonlinear effect and serious low-pass-like attenuation, etc. As a result, different probabilistic distributions may be required for the implementation of the PS technique, which increases the system's complexity.

In the literature, one classic and effective scheme named the adaptive modulation technique is widely used, which can boost the system's capacity [9]. Besides, a simplified

scheme named the pre-emphasis (or pre-equalization) technique was also widely used to effectively compensate for power fading in transmission systems [10]. However, the traditional adaptive loaded-DMT or pre-emphasis technique is channel-dependent and requires the channel state information (CSI) with the reverse link, which is complex and time consuming. Nowadays, a channel-independent precoding scheme is seen as another effective way to compensate for unbalanced impairments. Thus, by employing this technique, only one symbol modulation scheme and one kind of CCMD are required in PS-enabled DMT transmission systems. Some precoding matrices such as the Walsh–Hadamard transform (WHT) matrix [11], constant amplitude zero autocorrelation sequence (CAZAC) matrix [12], and discrete Hartley transform (DHT) matrix [13] have been employed to realize precoding for DMT transmission systems. The precoding technique can also be applied to reduce the peak-to-average power ratio (PAPR) owing to the improvement of the autocorrelation performance of signal symbols [14], and mitigate nonlinear distortions induced by electrical/optical devices. In [15], J. Ma et al. proposed and experimentally demonstrated an orthogonal circular matrix transform (OCT)-based precoding scheme in a short-reach IM-DD transmission system, which can effectively reduce the PS-enabled transceiver implementation complexity. Moreover, the precoding schemes based on seven commonly precoding matrices were comparatively investigated [16], and their computational complexities were theoretically analyzed and compared as well. It also indicated that, compared with other precoding matrices (e.g., OCT, DHT, CAZAC, etc.), there is no need for multiplication operations in WHT precoding, which can be considered as a suitable scheme to compensate unbalanced impairments in an optical IM-DD system regarding the computational complexity.

In the above-mentioned precoding works, all of the data-carrying SCs in DMT or OFDM symbols are used for precoding, and we call this method full data-carrying SC precoding (FDSP). Since the Hermitian symmetry (HS) constraint is required for the inverse fast Fourier transform (IFFT) to obtain the real-valued DMT signal, the number of data-carrying SCs is generally not an integer power of two. In this case, the precoding techniques cannot be directly implemented with the corresponding FFT-based fast algorithms. Moreover, when a large number of SCs are employed for data delivery, the FDSP exhibits high complexity from a hardware implementation point of view. To deal with this issue, the multi-band OCT-based precoding technique was proposed [17]. In addition, a block precoding (BL) scheme, in which the data-carrying SCs are divided into several groups and the number of data-carrying SCs in each group is an integer power of 2, was proposed in [18,19]. However, the difference in equalized SNRs is relatively large among these groups. Compared to the uniform modulation scheme, these methods need to adopt different modulation formats and probabilistic distributions according to the SNRs of groups.

In this work, to further reduce the implementation complexity of the precoding-enabled PS-DMT transceiver, a fast WHT-based partial data-carrying SC precoding (PDSP) technique is proposed and experimentally verified in the optical IM-DD transmission system. The proposed PDSP technique can realize SNR equalization and provide a significant reduction in implementation complexity. We also compare the proposed technique with the FDSP and digital pre-equalization techniques. The rest of this paper is structured as follows. The operation principle of the probabilistically shaping technique, fast WHT-based partial data-carrying SCs pre-coding (PDSP) scheme, and its computational complexity is described in Section 2. The experimental setup and verification are presented in Sections 3 and 4, respectively. The corresponding conclusion is finally summarized in Section 5.

2. Operation Principle

2.1. The Principle of PS Technique

The diagram for the PS technique is schematically plotted in Figure 1. At the transmitter, the upper (or lower) data sequence is separated into two bit streams, which contain V_1

and V_2 bits, respectively. The upper (or lower) data sequence is shaped to non-uniform distributed symbols (U_1) through CCDM, and its corresponding rate can be expressed as $R_{DM} = V_1/U_1$. In this scheme, the non-uniform distribution P_X is applied and can be expressed as [20]

$$P_X(x) = e^{-\lambda|x^2|} / \sum_{x \in \chi} e^{-\lambda|x^2|} \tag{1}$$

where λ is a rate parameter and these shaped symbols (M -PAM) can be expressed as $\chi = \{\pm 1, \pm 3, \dots \pm (M - 1)\}$. In this work, M is chosen to 8. Subsequently, these shaped symbols are mapped into binary bit sequences with labeling by gray mapping and encoded by low-density parity-check (LDPC) code with the DVB-S.2 standard. Note that a bit-level interleaver is applied in our work to further improve the performance of FEC coding [15]. In the following, 2 one-dimensional M -PAM symbols are mapped in I/Q parts, respectively, to generate a two-dimension M^2 -QAM symbol. Thus the information rate (IR) of PS-enabled 64-QAM (bits /QAM symbols), R_{PS} , can be expressed as

$$R_{PS} = 2(1 + R_{DM} - m(1 - R_C)) \tag{2}$$

where R_C is the rate of LDPC code and $m = \log_2 M$.

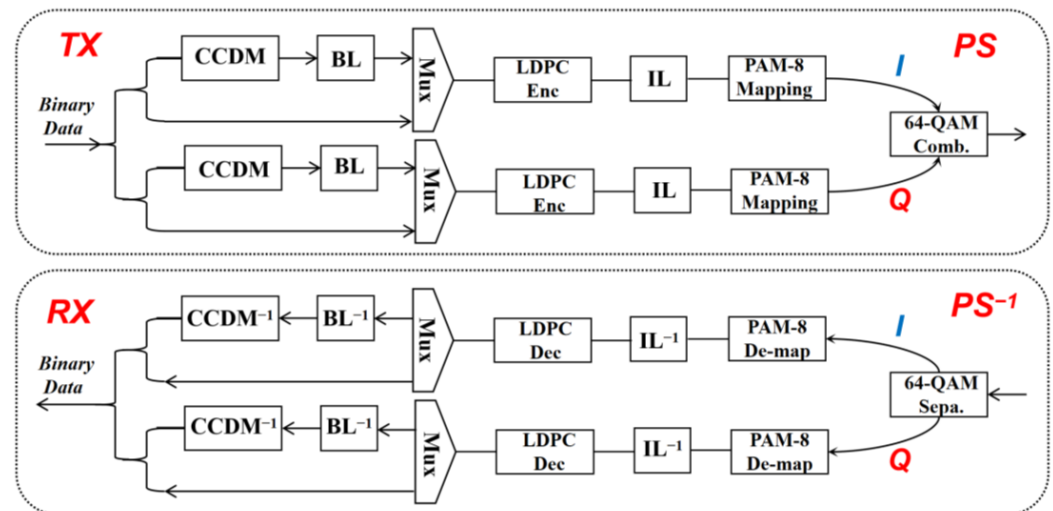


Figure 1. Schematic diagram of the PS-enabled DMT system.

At the receiver, the corresponding inverse operations for the PS technique are also shown in Figure 1. It should be mentioned that the generalized mutual information (GMI) under bit-metric decoding (BMD) is estimated by using log-likelihood ratios (LLRs) [7]. Assuming that N -points samples are obtained with the Monte Carlo simulation method, the GMI for I/Q parts can be written as [21]

$$GMI_{I(Q)} \approx \frac{1}{N} \sum_{k=1}^N (-\log_2 P_X(x_k)) - \frac{1}{N} \sum_{k=1}^N \sum_{i=1}^m \left(\log_2 \left(1 + e^{(-1)^{b_{k,i}} L_{k,i}} \right) \right) \tag{3}$$

where $b_{k,i}$ and $L_{k,i}$ represent the input bit and output bit, respectively. According to Equation (3), GMI_I and GMI_Q have the same calculation method, and the total GMI for the M^2 -QAM symbol equals to $GMI_I + GMI_Q$.

2.2. Fast WHT-Based PDSP Scheme

Ideally, only one probability distribution is required for the PS-DMT transmission system with a small range of SC SNR variations. However, the SC SNR may be largely fluctuated due to the imperfect frequency response of the optical/electrical devices, as illustrated in Figure 2a. In the conventional FDSP case, all of the data-carrying SCs are

regarded as one group and used for performing precoding (see Figure 2b,c). As mentioned above, the number of data-carrying SCs (F) is usually not an integer power of two due to the HS constraint. Thus, the hardware implementation of the FDSP is a big challenge when a large FFT size is applied for DMT modulation/demodulation. For the proposed PDSP scheme, we divide F data-carrying SCs into two groups: P data-carrying SCs in group 1, where P is a number of an integer power of two, on both sides are selected for precoding, while no precoding is performed for the left $F-P$ data-carrying SCs in group 2, as shown in Figure 2d,e. Note that the P data-carrying SCs selected from the successive data-carrying SCs in high/low-frequency whose SNRs are lower than average SNR and successive low-frequency data-carrying SCs with highest SNRs. In this case, the implementation complexity can be further reduced with the PDSP scheme in the PS-DMT transmission system.

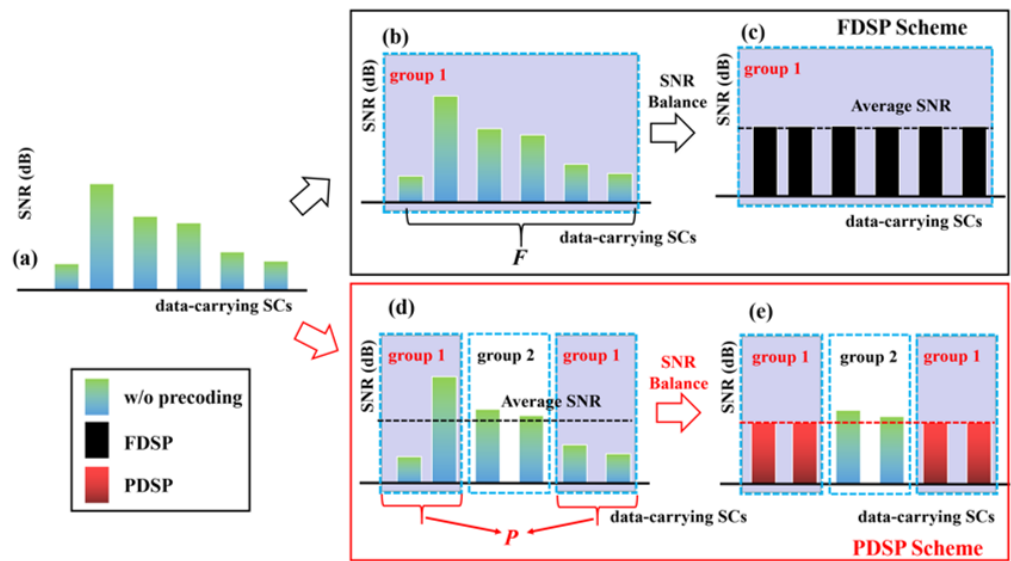


Figure 2. Schematic diagram of the PDSP scheme in the PS-enabled DMT system. (a) original SCs SNR, (b) SCs selected for FDSP, (c) SNR balance for FDSP, (d) SCs selected for PDSP and (e) SNR balance for PDSP.

Unlike other PDSP schemes with a complex-valued precoded matrix (e.g., DFT and OCT), the real-valued WHT-based PDSP technique has lower computational complexity. According to [16], the normalized Hadamard matrix of order P can be given by

$$D_P = \frac{1}{\sqrt{P}} \begin{bmatrix} D_{P/2} & D_{P/2} \\ D_{P/2} & -D_{P/2} \end{bmatrix}, D_2 = \frac{1}{\sqrt{2}} \begin{bmatrix} 1 & 1 \\ 1 & -1 \end{bmatrix} \quad (4)$$

where D_2 is the normalized Hadamard matrix of order 2, and P must be either 1, 2, or an integer multiple of 4. D_P can be constructed from D_2 . In the PDSP scheme, P is an integer number of two, the inverse matrix D_P^{-1} equals to D_P .

Once the PS is done, the shaped QAM symbols can be expressed as $X_F = [X_1, X_2, \dots, X_F]^T$ and $X_P = [X_1, X_2, \dots, X_P]^T$, where $F > P$ and T denotes the transpose operation. Thus, by multiplying the fast WHT-based precoding matrix D_P , the PDSP precoded symbols $Y_P = [Y_1, Y_2, \dots, Y_P]^T$ can be given by

$$Y_P = D_P X_P \quad (5)$$

After fiber channel transmission, without considering nonlinear distortions, the recovered PDSP symbols $R_P = [R_1, R_2, \dots, R_P]$ after FFT operation can be given by

$$R_P = H Y_P + W = H D_P X_P + W \quad (6)$$

The channel transfer matrix, H , is a diagonal matrix that can be expressed as $\text{diag}(h_1, h_2, \dots, h_P)$, and the frequency response of the k -th SC is h_k . Similarly, the noise on the k -th SC is denoted by W_k , which obeys Gaussian distribution with variance and zero mean. The corresponding noise vector in the frequency domain is expressed as $W = [W_1, W_2, \dots, W_P]$. Assuming that the accurate channel equalization is performed, the PDSP-decoded QAM symbols $Z_P = [Z_1, Z_2, \dots, Z_P]$ can be written as

$$Z_P = D_P^{-1}H^{-1}R_P = X_P + D_P^{-1}H^{-1}W = X_P + D_P H^{-1}W \tag{7}$$

After performing PDSP decoding, these data-carrying SCs can be treated equally and only one kind of CCDM and one symbol modulation scheme are required for the implementation of the PS-DMT transmission system.

2.3. Complexity Comparison

The computational complexities of FDSP/PSDP schemes are analyzed and listed in Table 1. The number of data-carrying SCs F is not an integer power of two in the WHT-based FDSP scheme, and the required real-valued addition operations may be resource-intensive. However, the fast WHT can be implemented when the number of precoded data-carrying SCs P is an integer power of two. Therefore, the computational complexity of the fast WHT-based PDSP scheme can be significantly reduced.

Table 1. WHT-based FDSP/PDSP computational complexity comparison.

Precoding Scheme	Refer to [16]		Fast Algorithm [18]	
	Real Mult.	Real Add.	Real Mult.	Real Add.
FDSP	0	$2F^2 - 2F$	-	-
PDSP	0	$2P^2 - 2P$	0	$2P\log_2(P)$

3. Experimental Setup

The experimental setup of the PS-DMT systems enabled by a fast WHT-based PDSP scheme is illustrated in Figure 3. At the transmitter (Tx), the digital PS-DMT signal is generated offline with digital signal processing (DSP) approaches in Matlab. Firstly, the pseudo-random binary sequence (PRBS) is generated and then sent to the PS module, which is clearly mentioned in Section 2.1. After that, the shaped 64-QAM symbols are precoded with the proposed fast WHT scheme. Note that only 96 and 64 positive-frequency SCs are, respectively, used for FDSP and PDSP schemes, and other SCs are filled with zeros. After the HS operation, the cyclic prefix (CP) with a length of eight points is added for each 256-point inverse fast Fourier transform (IFFT) output to resist ISI. Additionally, one training symbol (TS) is inserted in the front of each PS-DMT frame to realize both timing synchronization and channel estimation [22]. Finally, the precoded PS-DMT signal is digitally clipped to combat the digital-to-analog converter (DAC)-induced quantization noise [23] and reduce PAPR. The analog electrical DMT signals are converted by using a Tektronix arbitrary waveform generation (AWG, AWG7122C). The corresponding sampling rate and the resolution for D/A conversion are 12-GSa/s and 10-bits, respectively. Note that the average signal power for traditional/FDSP/PDSP PS-enabled DMT signals are set to equal in this experiment. The converted electrical DMT signals are suppressed by a low-pass filter (LPF) and then amplified by a Mini-Circuits electrical amplifier (EA, ZX60-14012L-S+) with a bandwidth of ~6 GHz. The Mach-Zehnder modulator (MZM) works at the quadrature point to minimize the non-linear distortion. The wavelength and output power of the laser diode (LD) are 1550 nm and 11 dBm, respectively. Then, the 2.5 dBm optical PS-DMT signals are coupled into a 50 km single-mode fiber (SMF), and its dispersion and loss are ~17 ps/nm/km and ~0.2 dB/km, respectively. At the receiver (Rx), the optical PS-DMT signal is attenuated by a variable optical attenuator (VOA). An optical coupler (OC) is used to change the received optical power (ROP). Then, the output PS-DMT signal with 90% power is detected by a photodiode (PD). The recovered

signal is amplified by an EA and captured by a digital storage oscilloscope (DSO, Lecroy Wavemaster 820-Zi-A, Teledyne LeCroy, Chestnut Ridge, New York, USA). The sampling rate of DSO and resolution for A/D conversion are 40 GSa/s and 8 bits, respectively. The sampled signals are post-processed with the Rx DSP flow, which consists of symbol timing synchronization, remove CP, FFT, ISFA-enhanced channel estimation [23], frequency domain equalization, fast WHT decoding, and PS demodulation. Finally, the different BER or GMI performances are calculated.

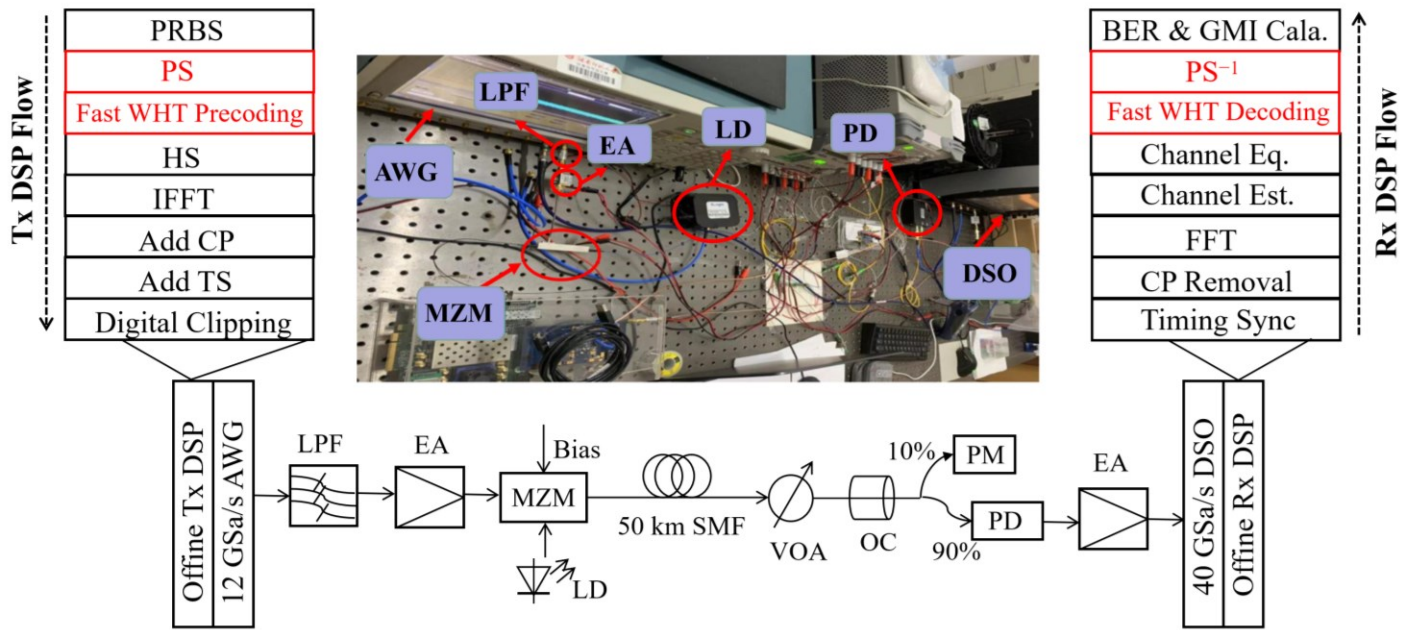


Figure 3. Experimental setup of the PS-DMT system enabled by fast WHT-based PDSP scheme.

When the rate of LDPC is set to 9/10, the different rates of CCDM, i.e., 1.75, 1.55 and 1.25 bits per one-dimensional symbol are discussed in this work. Therefore, according to Equation (2), the corresponding information rates (IRs) are 4.9, 4.5, and 3.9 per two-dimensional symbol (bits/QAM symbol). Meanwhile, the constellations of the three probability distributions for probabilistically shaped 64-QAM are also given in Figure 4. It shows clearly that, as the R_{DM} decreases, the probabilistically shaping for the DMT symbol can become more obvious. The bandwidth of the 64-QAM PS-DMT signal is constantly equal to 4.5 ($(96 \times 12)/256$) GHz. When the IR equal to 4.9 bits/QAM symbol, the corresponding data rate and net data rate are 22.05 ($12 \times 4.9 \times (96/256)$) Gb/s and 21.36 ($12 \times 4.9 \times (96/256) (900/901)$) Gb/s, respectively. Thus, the achievable spectral efficiency of the PS-DMT signal is 4.74 (21.36/4.5) bit/s/Hz. The key parameters of the precoded PS-DMT frame are indicated in Table 2.

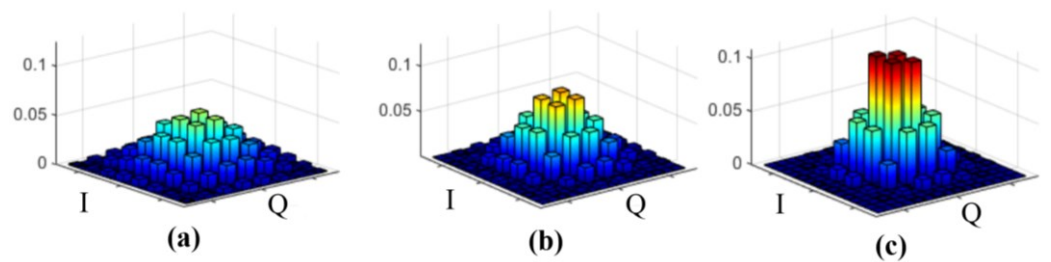


Figure 4. The constellations of the three probability distributions for probabilistically shaped 64-QAM. (a) $R_{DM} = 1.75$, (b) $R_{DM} = 1.55$ and (c) $R_{DM} = 1.25$.

Table 2. Some key parameters of the precoded PS-DMT frame.

Parameter	Value		Unit
	FDSP	PDSP	
Modulation format	64 QAM		-
IFFT/FFT size	256		points
Data SCs	96		-
Data SCs for Precoding	96	64	-
CP length	8		-
TS per frame	1		-
DMT symbols per frame	900		-
Clipping ratio (CR)	13		dB
Bandwidth	4.5		GHz

4. Results and Discussion

The three pre-processing techniques including digital pre-equalization (Preq), WHT-based FDSP and fast WHT-based PDSP are compared for PS-DMT at three IRs regarding electrical spectra, SNR equalization, BER, and GMI performance.

4.1. Spectrum Analysis

The electrical spectra of the transmitted signals for original, digital Preq, WHT-based FDSP and fast WHT-based PDSP schemes are shown in Figure 5a–d, respectively. For the digital Preq scheme, to resist high-frequency attenuation, the mapped QAM symbols are multiplied by a pre-equalization factor via round-trip feedback. Therefore, as shown in Figure 5b, its high-frequency power is relatively high.

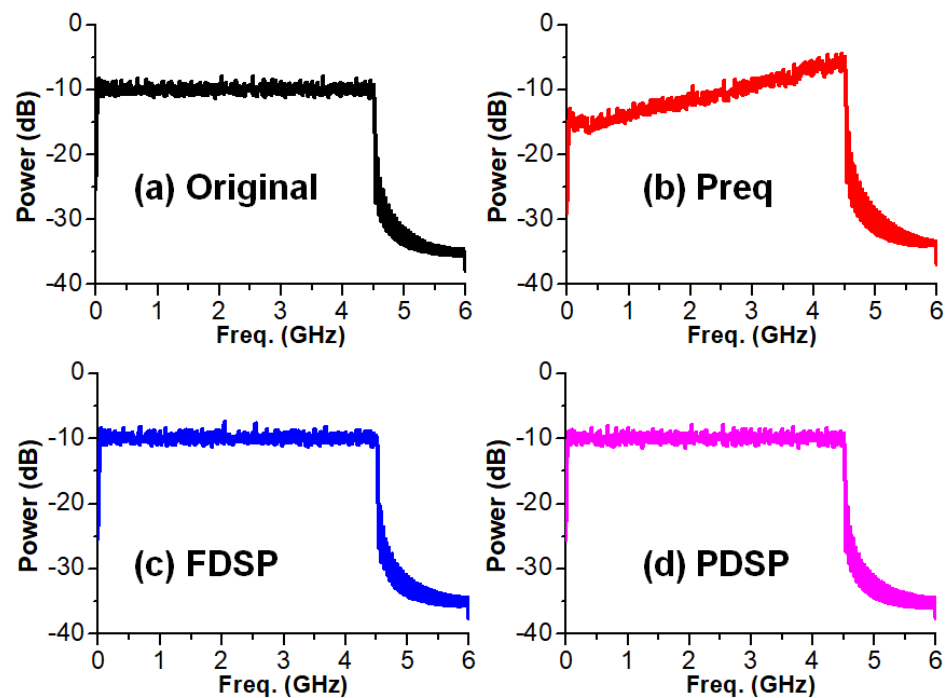


Figure 5. Spectral of the transmitted signals with (a) original scheme, (b) Preq scheme, (c) WHT-based FDSP scheme and (d) Fast WHT-based PDSP scheme.

After 50 km SMF transmission, the spectra of the received original, Preq, WHT-based FDSP and fast WHT-based PDSP precoded signals are shown in Figure 6a–d, respectively. Except for the Preq scheme, the high-frequency components of the spectra show obvious attenuation (see Figure 6a,c,d) owing to the low-pass filtering induced by the optical/electrical devices and fiber dispersions. The flat signal spectrum (see Figure 6b)

also indicates that the Preq scheme can compensate for the high-frequency attenuation of the PS-DMT signal in the IM-DD transmission system.

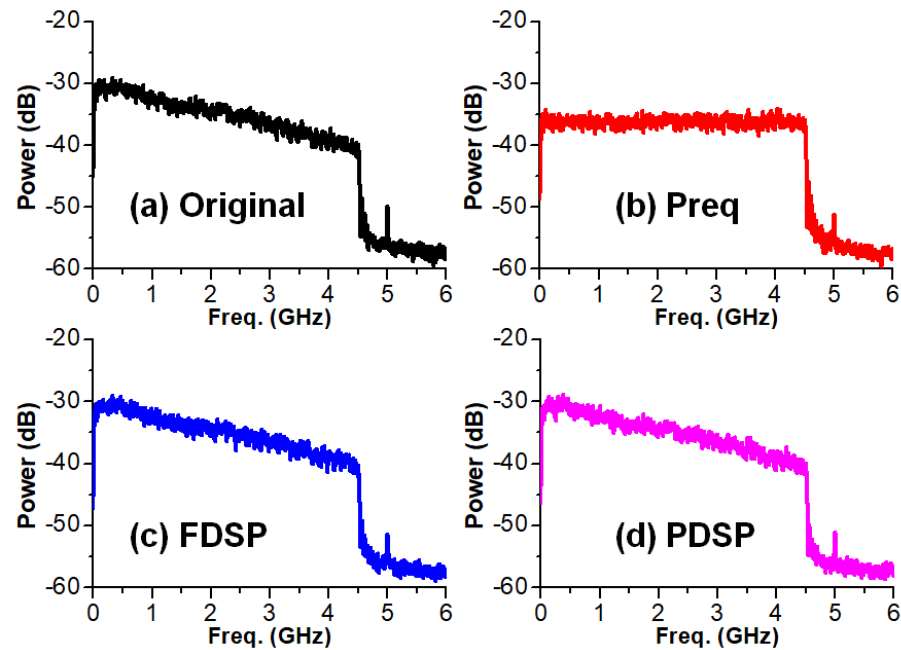


Figure 6. Spectra of the received signals with (a) original scheme, (b) Preq scheme, (c) WHT-based FDSP scheme and (d) Fast WHT-based PDSP scheme.

4.2. SNR Equalization

The estimated SC SNRs for four kinds of 64-QAM PS-DMT signals are shown in Figure 7, where the ROP and IR for the DMT symbols are -9 dBm and 4.9 bits/QAM, respectively. The SC SNR fluctuation is up to 13 dB for the original signal. The imperfect frequency response of the MZM and EA are the main reasons for low SNRs on the low-frequency SCs. Additionally, the degraded SNR on the high-frequency SCs is mainly caused by the bandwidth limitations of the optical/electrical devices and fiber dispersion. By using WHT-based FDSP or PDSP schemes, the SNR values on the precoded SCs are well equalized. Unlike the FDSP scheme, only 64 data-carrying SCs, with indices of 1st–32nd and 65th–96th, are used for the proposed PDSP scheme. Therefore, we can observe that the SNR value of the precoded SCs with the PDSP scheme is slightly lower than that of the FDSP scheme, but higher SNR performance on the middle data-carrying SCs with indices from 33rd to 64th is achieved with the PDSP scheme. Compared with the FDSP scheme, the Preq scheme can also play the role of equalizing the SC SNR.

When the ROP is set to -9 dBm, the recovered 64-QAM constellations for four kinds of PS-DMT signals are shown in Figure 8a–d. Compared to the conventional PS-DMT technique, the Preq, WHT-based FDSP and WHT-based PDSP schemes make the constellation points more distinct and convergent.

4.3. GMI and BER Performance

The GMI versus ROP for four different kinds of PS-DMT signal schemes at IRs of 4.9/4.5/3.9 bits/QAM symbol are investigated and shown in Figure 9a–c, respectively. They indicate that Preq, WHT-based FDSP and Fast WHT-based PDSP schemes have almost the same GMI performance and outperform the original one, due to the relatively flat SNR distribution. As the theoretical maximum information rate can be given by GMI with an ideal FEC code, there is about 0.3 dB improvement for the receiver sensitivity in PS-DMT transmission system with the LDPC rate of 9/10.

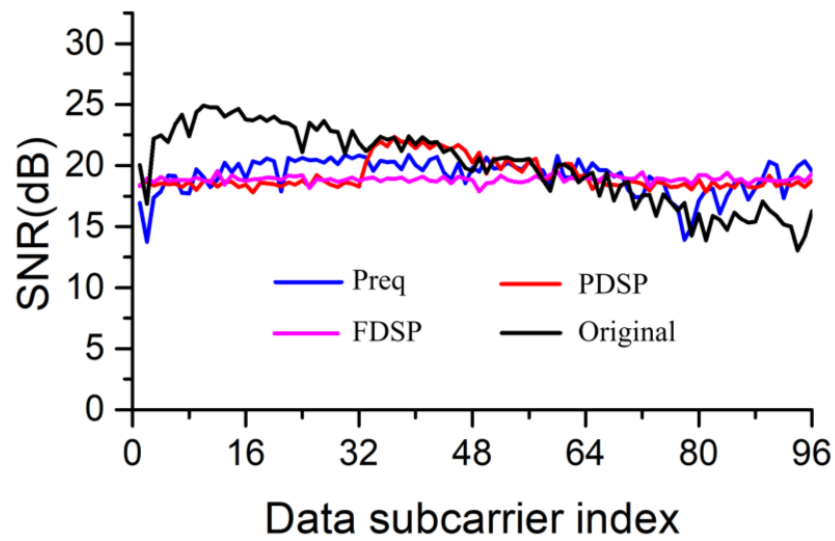


Figure 7. The estimated SC SNR for four kinds of received PS-DMT signals.

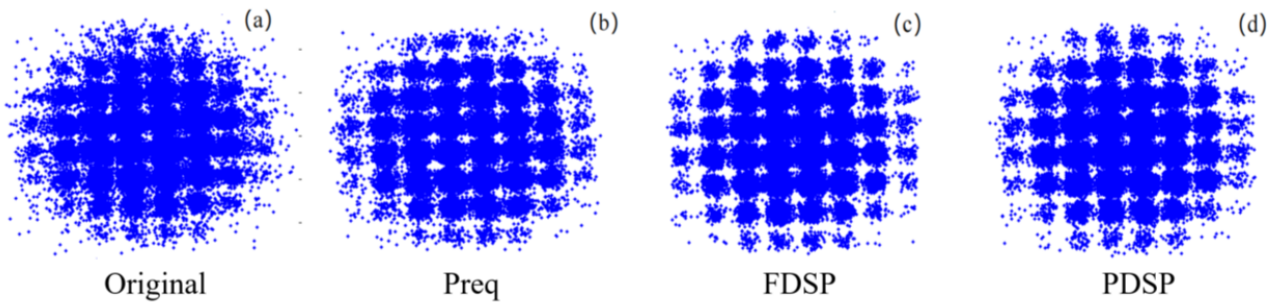


Figure 8. The recovered 64 QAM constellations for (a) original scheme, (b) pre-equalization, (c) WHT-based FDSP and (d) fast WHT-based PDSP.

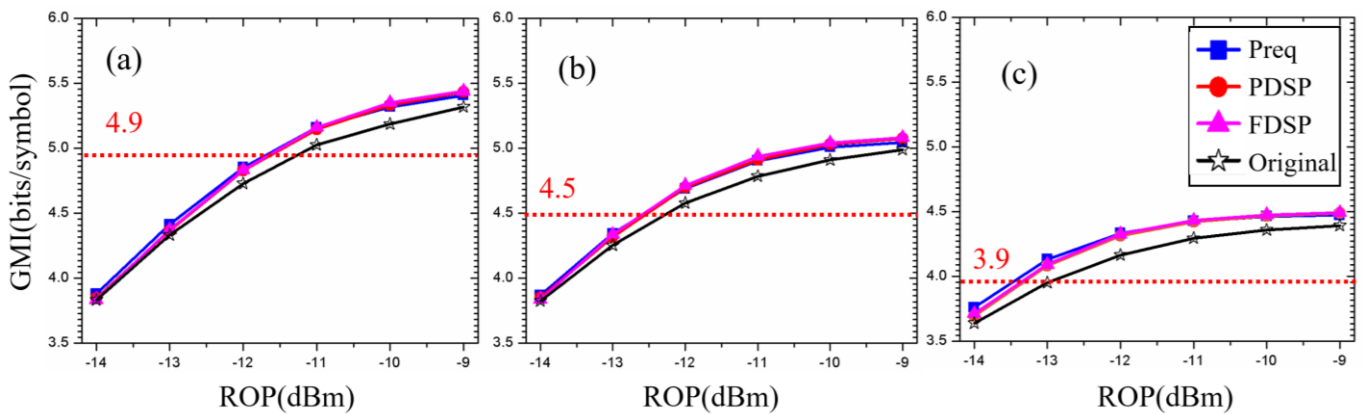


Figure 9. Measured GMI versus ROP for IRs of (a) 4.9, (b) 4.5 and (c) 3.9 bits/QAM symbol.

The measured BER performance for four kinds of PS-DMT signal scheme versus ROP is investigated and shown in Figure 10. When the LDPC rate is set to 9/10 and IRs equal to 4.9/4.5/3.9 bits/QAM symbol, compared with the original scheme, the receiver sensitivity improvements of about 1 dB can be achieved at BER performance below $1e-3$ for Preq/WHT-based FDSP/fast WHT-based PDSP schemes. Thus, the fast WHT-based PDSP scheme may be a good option for the implementation of the PS-DMT transmission systems with a large SC SNR fluctuation regarding computational complexity.

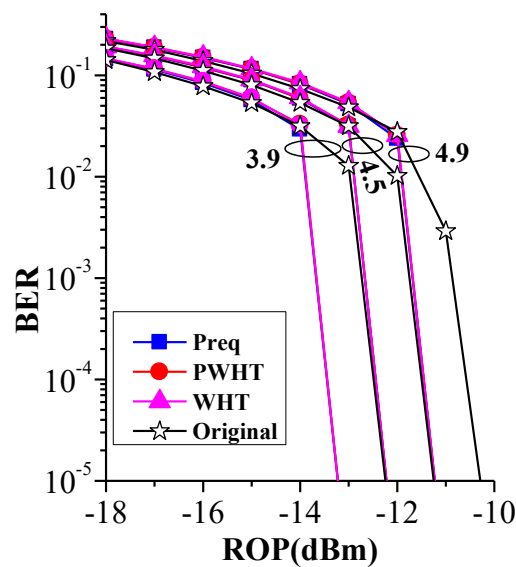


Figure 10. Measured BER performance for four kinds of PS-DMT signals versus ROP.

5. Conclusions

In this paper, we proposed and experimentally investigated a low-complexity fast WHT-based PDSP scheme to combat the unbalanced impairments and reduce the implementation complexity of PS-enabled DMT IMDD transmission systems. After 50 km SMF transmission, the results show that pre-equalization, WHT-based FDSP and fast WHT-based PDSP schemes have almost the same BER and GMI performance. Compared with the traditional PS-enabled scheme, there is about 1 dB gain for receiver sensitivity by employing the three pre-processing schemes. However, the proposed fast WHT-based PDSP scheme is a lower-complexity option for the implementation of the PS-DMT systems with large SC SNR fluctuation.

Author Contributions: Conceptualization, Y.L. and H.L.; methodology, Y.L., H.L. and M.C.; software and validation, Y.L. and H.L.; writing—original draft preparation, Y.L. and H.L.; review and editing, M.C. and T.Z.; supervision, M.C.; project administration, M.C. and Y.C.; funding acquisition, Y.C. All authors have read and agreed to the published version of the manuscript.

Funding: This work is supported by the Scientific Research Fund of Hunan Provincial Education Department of China under grants 20B330 and 21A0562, and the Construct Program of the Key Discipline in Hunan Province, China.

Institutional Review Board Statement: Not applicable.

Informed Consent Statement: Not applicable.

Data Availability Statement: Not applicable.

Conflicts of Interest: The authors declare no conflict of interest. The funders had no role in the design of the study; in the collection, analyses, or interpretation of data; in the writing of the manuscript, or in the decision to publish the results.

References

1. Nguyen, H.; Huang, S.; Wei, C.; Chuang, C.; Chen, J. 55-Gbps and 30-dB Loss Budget LR-OFDM PON Downstream Enabled by ANN-based Predistortion. In Proceedings of the 2021 Optical Fiber Communications Conference and Exhibition (OFC), San Francisco, CA, USA, 6–10 June 2021. paper M3G.4.
2. Li, F.; Li, X.; Chen, L.; Xia, Y.; Ge, C.; Chen, Y. High-level QAM OFDM system using DML for low-cost short reach optical communications. *IEEE Photon. Technol. Lett.* **2014**, *26*, 941–944.
3. Shi, J.; Zhang, J.; Zhou, Y.; Wang, Y.; Chi, N.; Yu, J. Transmission performance comparison for 100Gb/s PAM-4, CAP-16 and DFT-spread OFDM with direct detection. *J. Lightwave Technol.* **2017**, *35*, 5127–5133. [[CrossRef](#)]
4. Mei, J.; Li, K.; Ouyang, A.; Li, K. A profit maximization scheme with guaranteed quality of service in cloud computing. *IEEE Trans. Comput.* **2015**, *64*, 3064–3078. [[CrossRef](#)]

5. Fang, Y.; Yu, J.; Zhang, J.; Chi, N.; Xiao, J.; Chang, G.K. Ultrahigh-capacity access network architecture for mobile data backhaul using integrated W-band wireless and free-space optical links with OAM multiplexing. *Opt. Lett.* **2014**, *39*, 4168–4171. [[CrossRef](#)] [[PubMed](#)]
6. Buchali, F.; Steiner, F.; Böcherer, G.; Schmalen, L.; Schulte, P.; Idler, W. Rate adaptation and reach increase by probabilistically shaped 64-QAM: An experimental demonstration. *J. Lightwave Technol.* **2016**, *34*, 1599–1609. [[CrossRef](#)]
7. Böcherer, G.; Steiner, F.; Schulte, P. Bandwidth efficient and ratematched low-density parity-check coded modulation. *IEEE Trans. Commun.* **2015**, *63*, 4651–4665. [[CrossRef](#)]
8. Schulte, P.; Böcherer, G. Constant composition distribution matching. *IEEE Trans. Inf. Theory* **2016**, *62*, 430–434. [[CrossRef](#)]
9. Chen, X.; Feng, Z.; Tang, M.; Fu, S.; Liu, D. Performance enhanced DDO-OFDM system with adaptive partitioned precoding and single sideband modulation. *Opt. Express* **2017**, *25*, 23093–23108. [[CrossRef](#)] [[PubMed](#)]
10. Gao, Y.; Yu, J.; Xiao, J.; Cao, Z.; Li, F.; Chen, L. Direct-Detection Optical OFDM Transmission System With Pre-Emphasis Technique. *J. Lightwave Technol.* **2011**, *29*, 2138–2145. [[CrossRef](#)]
11. Deng, R.; He, J.; Chen, M.; Zhou, Y. Experimental demonstration of a real-time gigabit OFDM-VLC system with a cost-efficient precoding scheme. *Opt. Commun.* **2018**, *423*, 69–73. [[CrossRef](#)]
12. Feng, Z.; Wu, Q.; Tang, M.; Lin, R.; Wang, R.; Deng, L.; Fu, S.; Shum, P.P.; Liu, D. Dispersion-tolerant DDO-OFDM system and simplified adaptive modulation scheme using CAZAC precoding. *J. Lightwave Technol.* **2016**, *34*, 2743–2751. [[CrossRef](#)]
13. Ouyang, X.; Jin, J.; Jin, G.; Zhang, W. Low complexity discrete Hartley transform precoded OFDM for peak power reduction. *Electron. Lett.* **2012**, *48*, 90–91. [[CrossRef](#)]
14. Jiang, T.; Tang, M.; Lin, R.; Feng, Z.; Chen, X.; Deng, L.; Fu, S.; Li, X.; Liu, W.; Liu, D. Investigation of DC-biased optical OFDM with precoding matrix for visible light communications: Theory, simulations, and experiments. *IEEE Photonics J.* **2018**, *10*, 7906916. [[CrossRef](#)]
15. Ma, J.; He, J.; Wu, K.; Chen, M. Performance enhancement of probabilistically shaped OFDM enabled by precoding technique in an IM-DD system. *J. Lightwave Technol.* **2019**, *37*, 6063–6071. [[CrossRef](#)]
16. Chen, M.; Wang, L.; Xi, D.S.; Zhang, L.; Zhou, H.; Chen, Q.H. Comparison of different precoding techniques for unbalanced impairments compensation in short-reach DMT transmission system. *J. Lightwave Technol.* **2020**, *38*, 6202–6213. [[CrossRef](#)]
17. Hong, Y.; Xu, J.; Yeh, L.K.C.C.H.; Liu, L.Y.; Chow, C.W. Experimental investigation of multi-band OCT precoding for OFDM-based visible light communications. *Opt. Express* **2017**, *25*, 12908–12914. [[CrossRef](#)] [[PubMed](#)]
18. Wang, L.; Chen, M.; Chen, G.; Deng, A.; Zhou, H.; Liu, Y.; Cheng, Y. Fast WHT-based block precoding for DMT transmission. In Proceedings of the Asia Communications and Photonics Conference, Shanghai, China, 24–27 October 2021. paper W4B.6.
19. Li, F.; Xiao, X.; Li, X.; Dong, Z. Real-Time Demonstration of DMT-based DDO-OFDM Transmission and Reception at 50 Gb/s. In Proceedings of the 39th European Conference and Exhibition on Optical Communication (ECOC 2013), London, UK, 22–26 September 2013. paper 1–3.
20. Cho, J.; Winzer, P.J. Probabilistic constellation shaping for optical fiber communications. *J. Lightwave Technol.* **2019**, *37*, 1590–1607. [[CrossRef](#)]
21. Fehenberger, T.; Alvarado, A.; Böcherer, G.; Hanik, N. On probabilistic shaping of quadrature amplitude modulation for the nonlinear fiber channel. *J. Lightwave Technol.* **2016**, *34*, 5063–5073. [[CrossRef](#)]
22. Liu, Y.; He, J.; Chen, M.; Xiao, Y.Q.; Cheng, Y. 64APSK Constellation Scheme for Short-Reach DMT with ISDD Enabled SFO Compensation. *Opt. Commun.* **2020**, *467*, 125689. [[CrossRef](#)]
23. Chen, M.; He, J.; Fan, Q.; Dong, Z.; Chen, L. Experimental Demonstration of Real-Time High-Level QAM-Encoded Direct-Detection Optical OFDM Systems. *J. Lightwave Technol.* **2015**, *33*, 4632–4639. [[CrossRef](#)]